Large Magnetoresistance of Electrodeposited Single-Crystal Bismuth Thin Films

F. Y. Yang,[1] Kai Liu,[1] Kimin Hong,[1] D. H. Reich,[1] P. C. Searson,[2] C. L. Chien[1]*

Single-crystal bismuth thin films 1 to 20 micrometers thick were fabricated by electrodeposition and suitable annealing. Magnetoresistance up to 250 percent at 300 kelvin and 380,000 percent at 5 kelvin as well as clean Shubnikov–de Haas oscillations were observed, indicative of the high quality of these films. A hybrid structure was also made that showed a large magnetoresistive effect of 30 percent at 200 oersted and a field sensitivity of 0.2 percent magnetoresistance per oersted at room temperature.

Bismuth (Bi) is a semimetal with unusual electronic properties that result from its highly anisotropic Fermi surface, low carrier concentrations, and small effective carrier masses m^*. Because of its large Fermi wavelength and long carrier mean free path l (*1*), Bi has been extensively investigated for quantum transport and finite-size effects (*2, 3*). The small values of m^* and the very large value of l also produce the very large magnetoresistance (MR) effects observed in bulk single crystals of Bi (*4*) and recently in Bi nanowires (*5, 6*). The MR is $r(H) = [\rho(H) - \rho(0)]/\rho(0) \times 100\%$, where H is the magnetic field and ρ is the resistivity. Despite this, fabrication of high-quality Bi thin films, a requirement for studying Bi's transport properties and for technological applications such as magnetic field sensing (*7*), has been difficult. For example, Bi thin films made by evaporation and sputtering are often polycrystalline with small grains (*8*) and show MR that is typically orders of magnitude smaller than those of single crystals. Only very recently have high-quality Bi thin films been produced by using molecular beam epitaxy (MBE) onto BaF_2 substrates (*3, 9*), a well-controlled but costly and slow fabrication technique.

We report on the electrodeposition of high-quality, single-crystal Bi thin films that exhibit very large MR effects. Electrodeposition is intrinsically fast and compatible with patterning and large-scale production. We fabricated trigonal-axis-oriented, single-crystal Bi thin films that exhibit MR of as much as 380,000% at temperature $T = 5$ K and 250% at room temperature with a nonhysteretic and quasi-linear field dependence. The high quality of the Bi films is further illustrated by the observation of clean Shubnikov-de Haas oscillations at low T. We also demonstrate a simple hybrid structure with a large MR effect of 30% at 200 Oe and a field sensitivity of 0.2% MR per oersted at room temperature. These electrodeposited Bi thin films are new media suitable for studying the unusual transport properties of Bi and for the development of field-sensing devices.

The Bi thin films were electrodeposited from aqueous solutions of $Bi(NO_3)_3 \cdot 5H_2O$. The lateral dimensions of the films are defined by a thin Au underlayer (~100 Å thick) patterned onto a Si(100) wafer. The Au underlayer serves as the working electrode in a standard three-electrode electrodeposition cell, which also includes a Pt counterelectrode and a $Ag^+/AgCl$ reference electrode. Polycrystalline Bi films of thickness $t = 1$ to 20 μm deposited at a rate of ~0.2 μm/min have large grains (0.1 to a few micrometers), but after suitable annealing (268°C for 6 hours in Ar), they become single crystals, with the trigonal axis orientated perpendicular to the film plane. X-ray diffraction patterns of annealed films exhibit only the (003), (006), and (009) peaks (Fig. 1A). Pole-figure measurements of the (116) peaks show the expected sixfold symmetry (Fig. 1B). We also measured the pole-figures of the (202) and (012) peaks, both of which exhibit a threefold symmetry.

We measured the transport properties of the Bi films with a conventional four-probe method on samples of lateral dimensions 6 mm by 2 mm with the current in the long direction. We first examine the zero-field resistivity $\rho(0)$ and its T dependence for polycrystalline and single-crystal Bi films of various thicknesses. At $T = 5$ K, $\rho(0)$ for the polycrystalline films is dominated by grain-boundary scattering and hence is larger in the thinner films, which have smaller grains (Fig. 2A). For the single-crystal films, $\rho(0)$ is much lower (Fig. 2B) because grain-boundary scattering is eliminated. Because $l \gg t$, we are in the realm of finite-size effects, where scattering of carriers from the film surface significantly influences ρ. With carrier concentrations of $n = p = 3.7 \times 10^{17}$ cm^{-3} (n is the electron concentration and p is the hole concentration) determined from Hall effect measurements at 5 K, we determined from $\rho(0)$ the effective mean free path l_{eff}. For the single-crystal films with $t = 1$, 2, 5, 10, and 20 μm, the values of l_{eff} are respectively 2.9, 3.5, 4.7, 6.6, and 11 μm.

The MR was measured for magnetic fields H up to 5 T applied perpendicular to the film plane, and in the film plane either parallel (longitudinal) or perpendicular (transverse) to the current. As shown in Fig. 2, $\rho(5T)$ is many times larger than $\rho(0)$, and thus huge MR effects are observed. Because $\rho(0)$ is smaller and $\rho(5T)$ is much larger for the single-crystal films than for the polycrystalline films, the MR $r(H)$ of the single-crystal films is up to two orders of magnitude greater than that of the polycrystalline films. For example, in the 10-μm-thick polycrystalline film $r(5T) = 2100\%$ at 5 K, whereas in the 10-μm-thick single-crystal film $r(5T) = 153{,}000\%$.

The MR effect in Bi is the so-called ordinary MR, caused by the curving of the carrier trajectories in a magnetic field. The size of this effect is determined by $\omega_c\tau$, where $\omega_c = eH/m^*c$ is the cyclotron frequency and τ the relaxation time, which is proportional to l (e is the electron charge, m^* is the effective carrier mass, and c is the speed of light). At a given value of H, the value of ω_c is an intrinsic property of a given material. Be-

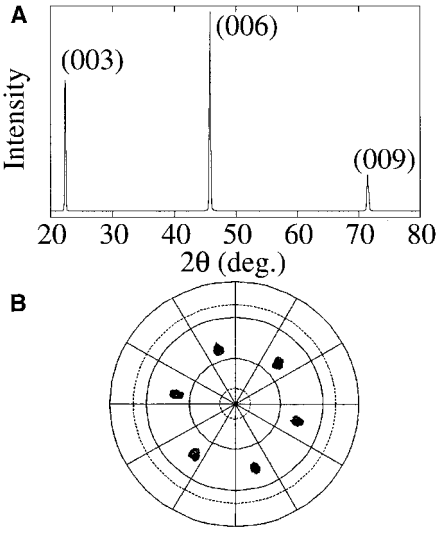

Fig. 1. X-ray diffraction patterns of a 5-μm-thick single-crystal Bi film. (**A**) The θ-2θ scan shows that the film is oriented along the trigonal axis. (**B**) Pole-figure scan of the (116) peaks exhibits the expected sixfold symmetry, where the radial direction is the tilt angle ψ between the normal direction of the film and the diffraction plane (0° to 90°), and the angular direction is the rotation angle Φ (0° to 360°).

[1]Department of Physics and Astronomy, [2]Department of Materials Science and Engineering, The Johns Hopkins University, Baltimore, MD 21218, USA.

*To whom correspondence should be addressed.

cause m^* is much smaller in Bi than in common metals, ω_c is about two orders of magnitude larger. The key to realizing a large MR effect in Bi films is the long l (equivalently a large τ), which is directly related to the sample quality. Most evaporated and sputtered Bi films have small grain sizes and show very small MR effects, orders of magnitude smaller than even those of the polycrystalline Bi films reported here (*8*). We note that the MR of our 2-μm-thick single-crystal electrodeposited Bi films is the same as that of 2-μm-thick MBE-grown films, which are the thickest such films reported (*9*).

For single-crystal films, ρ(5T) increases rapidly as T decreases from 300 K because of the rapid growth of l (as well as $\omega_c\tau$) (Fig. 2B). The small maxima in the ρ(5T) curves of the single-crystal films at low T stem from the delicate balance between the T dependence of n (and p) and l in a thin film.

The H dependence of ρ and of the MR for polycrystalline and single-crystal 20-μm-thick Bi films at 5 K is shown in Fig. 3. The perpendicular MR is always the largest and the longitudinal MR the smallest because of the orientation of the cyclotron orbits in the different measuring geometries parallel and perpendicular to the film plane, respectively. For both the polycrystalline and single-crystal Bi films, the H dependence of the perpendicular and transverse MR is quasi-linear and nonhysteretic and does not saturate in the field range probed. However, for the single-crystal Bi films, there are Shubnikov-de Haas (S-dH) oscillations superimposed on the MR in all three geometries. For a 10-μm-thick film measured up to H = 9 T, the MR changes little below 4 K, but the amplitude of the oscillations increases with decreasing temperature (Fig. 4A). The S-dH oscillations can be shown more clearly by subtracting the MR data at 4 K from that at 0.06 K. More than eight S-dH oscillations are observed, which are periodic in $1/H$ (Fig. 4B). Oscillations of this type reflect periodic, field-dependent modulations in the electronic density of states as successive, quantized cyclotron orbits become commensurate with extremal orbits on the Fermi surface (*10*). The details of the S-dH oscillations in all geometries will be discussed elsewhere (*11*).

Of particular interest for technological applications is the MR effect at room temperature. This is much smaller than the MR at low T because of the greatly reduced mean free path, but nonetheless a very large MR still remains. The MR at room temperature is between 200 and 300% (sputtered Bi films show 1% MR at room temperature) and is roughly the same for all of the electrodeposited films studied in both the perpendicular and transverse orientations. The MR of r(5T) = 250% for the 20-μm-thick Bi films at 300 K is greater than the largest giant magnetoresistance (GMR) observed at any temperature (*12*). The nonhysteretic MR of the Bi films, which increases quasi-linearly with field in a manner analogous to the Hall effect, can potentially be used for wide-range field and current sensors. Although it remains to be seen how Bi-based MR devices might ultimately compare to other wide-range devices, one advantage they should have over Hall effect sensors is the ability to measure fields in different orientations relative to the device without loss of sensitivity.

The original GMR effect in magnetic nanostructures arises from spin-dependent scattering and occurs only at large magnetic fields, but spin valves and other structures allow it to be useful for detecting smaller fields (*13*). With suitable hybrid structures, the large intrinsic MR effect in electrodeposited Bi can also be used to detect small magnetic fields. By using the strong response at small H of a soft magnetic material such as Fe, a large MR effect can be observed in a Bi sensing element placed near the edge of the soft magnetic material, where a large local magnetic field exists. A simple hybrid sensor involving an electrodeposited Bi film and small Fe slabs registers a MR effect of 6000% at 5 K and 30% at room temperature at H = 200 Oe. The field sensitivity is ~0.2% MR/Oe from 50 to 200 Oe at room temperature.

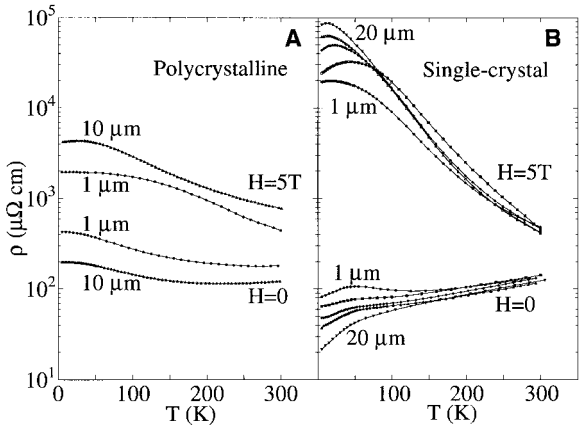

Fig. 2. Temperature dependence of ρ(0) and perpendicular MR at 5 T [ρ(5T)] of (**A**) representative polycrystalline 1-μm- and 10-μm-thick Bi films and (**B**) single-crystal films 1 to 20 μm thick. In (B), the curves at low T are in decreasing [ρ(0)] and increasing [ρ(5T)] order for thickness t = 1, 2, 5, 10, and 20 μm.

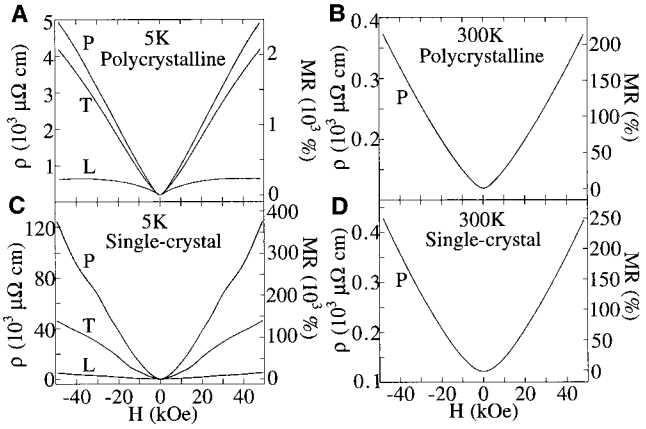

Fig. 3. The MR of a 20-μm-thick electrodeposited Bi film: (**A**) as-deposited polycrystalline film at 5 K in the perpendicular (P), transverse (T), and longitudinal (L) geometries; (**B**) as-deposited film at 300 K in the P geometry; (**C**) single-crystal film at 5 K in the P, T, and L geometries; and (**D**) single-crystal film at 300 K in the P geometry.

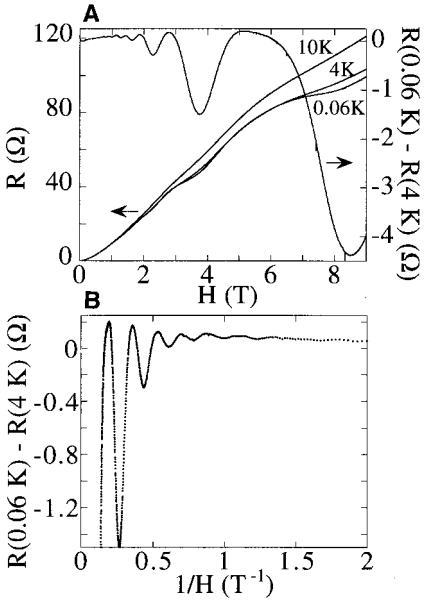

Fig. 4. (**A**) Field dependence of resistance (R) in the perpendicular geometry of a 10-μm-thick Bi film at 10 K, 4 K, and 0.06 K and the S-dH oscillations shown by R(0.06 K) − R(4 K). (**B**) The S-dH oscillations are shown to be periodic in $1/H$.

References and Notes

1. G. E. Smith, G. A. Baraff, J. M. Rowell, *Phys. Rev.* **135**, A1118 (1964).
2. Yu. F. Komnik, E. I. Bukhshtab, Yu. V. Nikitin, V. V. Andrievskii, *Zh. Eksp. Teor. Fiz.* **60**, 669 (1971) [*Sov. Phys. JETP* **33**, 364 (1971)].
3. M. Lu *et al.*, *Phys. Rev. B* **53**, 1609 (1996).
4. J. H. Mangez, J-P. Issi, J. Heremans, *Phys. Rev. B* **14**, 4381 (1976).
5. Kai Liu, C. L. Chien, P. C. Searson, Kui Yu-Zhang, *Appl. Phys. Lett.* **73**, 1436 (1998).
6. Z. Zhang, X. Sun, M. S. Dresselhaus, J. Y. Ying, J. P. Heremans, *Appl. Phys. Lett.* **73**, 1589 (1998).
7. G. A. Prinz, *Science* **282**, 1660 (1998).
8. D. E. Beutler and N. Giordano, *Phys. Rev. B* **38**, 8 (1988).
9. D. L. Partin *et al.*, *ibid.*, p. 3818.
10. N. W. Ashcroft and N. D. Mermin, *Solid State Physics* (Saunders, Philadelphia, 1976), chap. 14.
11. F. Y. Yang *et al.*, unpublished data.
12. R. Schad *et al.*, *Appl. Phys. Lett.* **64**, 3500 (1994).
13. B. Dieny *et al.*, *Phys. Rev. B* **43**, 1297 (1991); T. C. Anthony, J. A. Burg, S. Zhang, *IEEE Trans. Magn.* **30**, 3816 (1994).
14. Supported by NSF grants DMR96-32526 and DMR97-32763.

13 January 1999; accepted 9 April 1999

Cracks Faster than the Shear Wave Speed

A. J. Rosakis,* O. Samudrala, D. Coker

Classical dynamic fracture theories predict the surface wave speed to be the limiting speed for propagation of in-plane cracks in homogeneous, linear elastic materials subjected to remote loading. This report presents experimental evidence to the contrary. Intersonic shear-dominated crack growth featuring shear shock waves was observed along weak planes in a brittle polyester resin under far-field asymmetric loading. When steady-state conditions were attained, the shear cracks propagated at speeds close to $\sqrt{2}$ times the material shear wave speed. These observations have similarities to shallow earthquake events where intersonic shear rupture speeds have been surmised.

Over the past 50 years, fracture mechanics theories have had enormous success in predicting the failure of brittle materials, a class of materials that exhibit a linear elastic constitutive response up to failure. Cracks or fractures are displacement discontinuities in an otherwise intact material. On the basis of the nature of the displacement discontinuity near the crack tip, three distinct fracture modes can be defined: mode I, the in-plane opening mode resulting from normal separation of the crack faces (opening displacement discontinuity); mode II, the in-plane shearing mode resulting from relative sliding of crack faces perpendicular to the crack edge (sliding displacement discontinuity); and mode III, the anti-plane shearing mode resulting from relative out-of-plane sliding of the crack faces (tearing displacement discontinuity).

Griffith's energy balance criterion states that if the body can supply sufficient energy per unit crack advance to the crack tip to create new surfaces, then crack initiation will take place. However, if a crack starts to propagate rapidly, inertial effects come into play and the kinetic energy of the material particles must be taken into account. Griffith's energy criterion is then appropriately modified to include the net flux of kinetic energy and elastic strain energy into a vanishingly small contour around the crack tip. As the crack tip speed is increased to the free surface or Rayleigh wave speed of the material, c_R, the net flux of energy into the propagating crack tip vanishes, thus making c_R the theoretical limiting crack tip speed (*1*). This speed is an upper bound for in-plane cracks in idealized continuum models without local length scales and structure. In real materials, experimentally observed crack tip speeds seldom exceed 40 to 50% of the Rayleigh wave speed even in the most brittle materials (*2, 3*). A variety of explanations, ranging from high strains (*4*) and micro damage zones around the crack tip (*3*) to wavy crack paths (*5*), have been offered to reconcile the discrepancy between the observed terminal speed and the theoretically determined limit.

Washabaugh and Knauss (*6*) proposed that the observed maximal speed of crack propagation is inherently related to the strength of the material. On the basis of earlier work by Ravichandar and Knauss (*3*), they argued that in amorphous brittle solids a zone of microcracks is generated around a propagating crack tip, which is responsible for substantially reducing the crack speed and eventually inducing crack tip branching. In their experiments, they suppressed the formation of microcracks and the tendency for branching by fabricating weak planes along which cracks were forced to propagate under remote, symmetric opening loading conditions. Along these weak planes they reported subsonic (speeds less than the shear wave speed, c_S) opening mode cracks with speeds asymptotically approaching $c_R \approx 0.92c_S$ in the limit of vanishing bond strength. In a laboratory setting, the only experimental observations of intersonic crack tip speeds (speeds between c_S and the dilatational wave speed, c_L) and supersonic crack tip speeds (speeds greater than c_L) have been limited to cases where the loading is applied directly at the crack tip. Winkler *et al*. reported supersonic crack growth along weak crystallographic planes in anisotropic single crystals of potassium chloride, where the crack tip was loaded by laser-induced expanding plasma (*7*). At an entirely different length scale, indirect observations of intersonic shear rupture have been reported for shallow crustal earthquakes (*8, 9*). Here the fault motion is primarily shear dominated, and the material is not strictly monolithic because preferred weak rupture propagation paths exist in the form of fault lines.

Motivated by the observations of highly dynamic shear rupture during earthquakes, a substantial analytical effort has been made to model the mechanics of both subsonic and intersonic dynamic shear crack propagation. Andrews (*10*) showed that a shear crack can have a terminal speed either less than c_R or slightly greater than $\sqrt{2}c_S$, depending on the cohesive strength of the fault plane ahead. Burridge *et al*. (*11*) concluded that the speed regime $c_S < v < \sqrt{2}c_S$ (where v is the crack tip speed) is inherently unstable for dynamic shear crack growth. Broberg (*12*) showed that the speed regime $c_R < v < c_S$ is forbidden for both opening and shear mode cracks, whereas the speed regime $c_S < v < c_L$ is forbidden for opening mode cracks only. Freund (*13*), on the basis of his asymptotic solution for a steady-state shear mode intersonic crack, concluded that $\sqrt{2}c_S$ is the only speed permissible for a stable intersonic shear crack. Broberg (*14, 15*) also solved the problem of an intersonic shear crack symmetrically expanding at constant speed from zero initial length. He allowed for the existence of a finite process region ahead of the tip and concluded that a shear crack can propagate at all intersonic speeds, except those close to c_S and c_L. He also discussed the importance of the speed $\sqrt{2}c_S$ within the assumptions of his model. All of these analytical studies constrained the shear crack to move along a prescribed straight-line path in its own plane. To our knowledge, direct experimental confirmation of intersonic shear crack growth has not yet been reported.

We sought to determine whether in-plane shear intersonic crack growth could be obtained in laboratory specimens under remote shear loading conditions. In monolithic, prenotched laboratory specimens subjected to shear loading, after initiation from the notch tip the crack does not follow a straight path in

Graduate Aeronautical Laboratories, California Institute of Technology, Pasadena, CA 91125, USA.

*To whom correspondence should be addressed. E-mail: rosakis@aero.caltech.edu